Received: 10 April 2020 | Revised: 28 May 2021 | Accepted: 6 June 2021

DOI: 10.1002/pip.3449

RESEARCH ARTICLE

PROGRESS IN PHOTOVOLTAICS WILEY

How band tail recombination influences the open-circuit voltage of solar cells

Max Hilaire Wolter[1] | Romain Carron[2] | Enrico Avancini[2,3] | Benjamin Bissig[2] | Thomas Paul Weiss[1,2] | Shiro Nishiwaki[2] | Thomas Feurer[2] | Stephan Buecheler[2] | Philip Jackson[4] | Wolfram Witte[4] | Susanne Siebentritt[1]

[1]Laboratory for Photovoltaics, Physics and Materials Science Research Unit, University of Luxembourg, Belvaux, Luxembourg

[2]Laboratory for Thin Films and Photovoltaics, Empa – Swiss Federal Laboratories for Materials Science and Technology, Dübendorf, Switzerland

[3]Faculty of Science and Technology, Free University of Bozen-Bolzano, Bolzano, Italy

[4]ZSW – Zentrum für Sonnenenergie- und Wasserstoff-Forschung Baden-Württemberg, Stuttgart, Germany

Correspondence
Max Hilaire Wolter, Laboratory for Photovoltaics, Physics and Materials Science Research Unit, University of Luxembourg, 41, rue du Brill, L-4422 Belvaux, Luxembourg.
Email: mawoltr@gmail.com

Funding information
Horizon 2020 Framework Programme, Grant/Award Number: 641004; Swiss State Secretariat for Education, Research and Innovation (SERI), Grant/Award Number: 15.0158

Abstract

The power conversion efficiency of solar cells strongly depends on the open-circuit voltage V_{OC} which, in turn, depends on the recombination activity within the device. A possible source of detrimental charge carrier recombination is band tails. An empirical linear relationship between V_{OC} loss and the Urbach energy of the band tails has been shown in the past. Here we discuss how band tails influence the radiative recombination and the nonradiative recombination in the bulk of the absorber. First, we show through photoluminescence that the band tails can be willfully tuned in state-of-the-art thin-film Cu (In,Ga)Se_2 (CIGSe) absorbers and solar cells on a 20% efficiency level and beyond through the incorporation of alkali atoms. In the second part, we compare our CIGSe results to published results from other solar cell technologies. This comparison reveals that CIGS solar cells follow the previously described empirical trend: an increase in the open-circuit voltage with decreasing band tails. Finally, we model the influence of tail states on the radiative and nonradiative recombination losses: Radiative recombination is increased because carriers thermalize into the tail states and nonradiative recombination of free carriers in the bands is increased because of Shockley–Read–Hall recombination through the tail states. The comparison with experimental data shows that the influence of tail states is even worse than the increase in radiative and SRH recombination predicted by our model. Our results thus suggest that band tails act as one of the main remaining voltage limitations in the majority of state-of-the-art solar cells.

KEYWORDS
band tails, Cu (In,Ga)Se_2, open-circuit voltage, solar cells, Urbach energy

1 | INTRODUCTION

The efficiency of a solar cell defines how much solar energy can be converted into electricity and strongly depends on the solar cell's open-circuit voltage V_{OC}. The latter is a quantity that is dictated by the charge carrier recombination activity within the semiconducting absorber of the solar cell. Ideally, the only recombination is radiative band-to-band recombination, which is an unavoidable and necessary process to keep the detailed balance in the ideal case. In real systems, however, several additional harmful recombination channels are

present and limit the V_{OC}. An improvement in the V_{OC} is generally achieved by reducing the harmful recombination processes. One potential cause of harmful recombination is band tails. Band tails are defined as a density of states (DOS) that extend from the bands into the band gap of a semiconductor and are caused by structural and thermal disorder.[1,2] The investigation of band tails has recently caught renewed attention in a wide variety of solar cell materials such as chalcopyrites[3], kesterites[4], perovskites[5–7], and quantum dot lead sulfides[8]. Furthermore, several studies reveal a correlation between band tails and the V_{OC}[5,6,8], which suggests a causal relationship. Consequently, as a source of voltage losses in solar cells, the charge carrier recombination activity through band tails appears to play a crucial role.

To identify the exact influence of the band tails on the open-circuit voltage, a material system is required where the band tails can be willfully tuned. An example of such a system is state-of-the-art Cu (In,Ga)Se_2 (CIGSe) thin-film solar cells where the band tailing can be manipulated by the addition of an alkali-based post-deposition treatment (PDT).[9] The alkali PDT is a process where alkali fluorides are deposited onto the surface of the absorber after growth. When done at elevated temperatures, the alkali atoms can diffuse into the absorber. While Rudman et al. introduced the alkali PDT already back in 2004 by using the light alkali element Na[10], the recent increases in efficiency from 20.3%[11] in 2011 to the current record efficiency of 23.35%[12] in early 2019 are due to the usage of the heavier alkali elements such as K[13], Rb[14], and Cs[14,15]. Even though the alkali PDT improves all solar cell parameters, a direct influence is distinguishable for the open-circuit voltage V_{OC}. The exact cause for the V_{OC} improvement is not yet clear and currently heavily debated.[16–20] An encompassing review of relevant literature can be found in ref[9], where the role of band tails for the V_{OC} loss was already pointed out.

In this contribution, we thoroughly investigate the band tails in state-of-the-art CIGSe absorbers grown in either a low-temperature (suitable for the deposition on flexible substrates) or a high-temperature co-evaporation process. A precise description of the samples is given in the experimental Section 2. As the alkali incorporation into the absorbers leads to a well-reported increase of the V_{OC} in both low- and high-temperature absorbers[14,21,22], we can use CIGSe as a reference system that allows us to monitor and quantify the influence of band tail recombination on the solar cell performance. Ultimately, this allows us to identify whether a change in the band tails is responsible for the observed increase in the V_{OC} and thus to declare if band tails merit the attention that they so prominently attract.

2 | EXPERIMENTAL

2.1 | Sample preparation

In total, nine different sets of CIGSe samples have been investigated in this study. This specific combination of various samples is selected to represent a broad range of preparation-specific methods such as growth conditions, substrates, and PDTs. Table 1 summarizes important selected sample properties. Absorbers that share a similar label (e.g., H1 and H2) have been grown at identical conditions but received a different PDT (or none at all). As such, the samples can be allocated into different groups:

- H1 and H2
- L1, L2, and L3
- LN1 and LN2
- LS and LC

The samples LS and LC are included as they represent highly efficient devices. The labeling letter "L" refers to a growth process at low temperatures, while the letter "H" designates samples that were grown at

TABLE 1 Selected properties of the samples that feature in this study

Sample	PDT	Presence of alkalis	CGI	E_g /eV	V_{OC} /V	Efficiency/ %
H1	RbF	Na & Rb	0.92	1.077	0.707	20.0
H2	None	Na	0.93	1.083	0.690	19.1
L1	NaF + RbF	Na & Rb	0.86	1.147	0.708	18.2
L2	NaF	Na	0.87	1.148	0.685	16.5
L3	None	None	0.87	1.142	0.581	13.3
LN1	NaF + RbF	Na & Rb	0.89	1.124	0.705	17.8
LN2	NaF	Na	0.90	1.137	0.689	16.5
LS	NaF + RbF	Na & Rb	0.94	1.129	0.716	19.2
LC	NaF + RbF	Na & Rb	0.96	1.000	0.611	18.4

Note: Indicated are the sample label, the PDT, the presence of alkalis within the absorber, the compositional [Cu]/([Ga] + [In]) (CGI) ratio, the band gap energy E_g, the open-circuit voltage V_{OC}, and the power conversion efficiency (without antireflective coating; typically the efficiencies can be increased around 1% absolute or even more by applying an anti-reflective coating). Safe for the band gap energy, the indicated values all represent averages across several solar cells (typically 6 to 10). The determination of the band gap energy is described in detail in the supporting section S1.

high temperatures. All samples are present as CdS-covered absorbers as well as finished solar cell devices without antireflective coating. More information about the preparation process as well as in-depth characterization of samples H1, H2, L1, L2, L3, LN1, LN2, and L2 can be found in refs.[9, 14, 23–26]. The preparation process of sample LC is detailed in ref.[27].

2.2 | Sample characterization

2.2.1 | Photoluminescence

Photoluminescence spectroscopy measurements are conducted at room temperature in a home-built setup that allows intensity calibration and spectral calibration. The samples are excited by 1.88 eV (660 nm) photons emitted from a diode laser. To mimic the total photon flux density of the AM1.5 sun spectrum, the incident laser photon flux density is set to $2.76 \cdot 10^{17}$ cm^{-2} s^{-1} and $3.00 \cdot 10^{17}$ cm^{-2} s^{-1}, depending on the band gap energy of the absorber (1.1 and 1.0 eV, respectively). The laser spot at the sample position measures 2.6 mm in diameter (determined by a CMOS camera). The emitted PL signal is gathered by two off-axis parabolic mirrors and redirected into a 303-mm focal length spectrometer. From the grating inside the spectrometer, the light is dispersed into a 512-element InGaAs array. Finally, the recorded PL signal is spectrally calibrated using the known spectrum of a commercial halogen lamp. Intensity-calibrated measurements are described in more detail in Section S2 of the supporting information and are used to determine the quasi-Fermi level splitting (QFLS) according to Planck's generalized law.[28,29] QFLSs values are presented in Section S4 of the supporting information. Once the QFLS is known, Planck's generalized law can be used to determine the absorptivity.[30,31] However, state-of-the-art Cu (In,Ga)Se_2 absorbers show generally interferences near and below the absorption edge.[32] These interferences do not disturb the determination of the QFLS[32,33], but they are particularly strong at low absorption and thus in the region of the tail states. We developed a reversible surface treatment to remove the interferences.[34,35] With this layer, we can no longer calibrate the intensity of the incoming or the outcoming light. However, the absorption of the layer is spectrally flat, that is, the spectral calibration is still reliable and allows to determine the spectral shape of the absorption, albeit not the absolute value. It is thus possible to determine Urbach energies from the absorption spectra as described in Section S2 of the supporting information. In this case of spectral calibration only, the incident photon flux is not equivalent to an AM1.5 spectrum.

2.2.2 | Current–voltage characterization

The solar cell parameters are determined from current–voltage measurements using an ABA-class solar simulator in a 4-probe configuration at 25°C and using a simulated AM1.5G spectrum with a Si cell for calibration.

2.2.3 | Compositional analysis

The average elemental composition of the samples is measured by using a 45-keV home-built X-ray fluorescence spectrometer. From the recorded spectra, the Kα peaks of the Cu, In, Ga, and Se species are fitted. The measured CGI ratios are believed to deviate from the real compositional ratio by less than 0.03 in absolute. The depth-dependent compositional measurements are carried out with a time-of-flight secondary ion mass spectrometer (ION-TOF GmbH TOF SIMS5) using the ions O_2^+ for sputtering and Bi^+ for analysis.

2.2.4 | External quantum efficiency

External quantum efficiency (EQE) measurements are used as a supporting tool for the definition of the band gap energies of the samples. The band gap determination is described in detail in Section S1 of the supporting information. The EQE measurements are done at 25°C with a white light halogen lamp as light source. The light is chopped at 270 Hz and split into its monochromatic spectral components in a LOT MSH-300 monochromator before reaching the solar cell subjected to a light bias of about 0.15 suns. A certified Si cell and a calibrated Ge cell are used to calibrate the intensity.

3 | URBACH-TYPE BAND TAILS IN CU(IN,GA)SE_2

Band tails consist of a DOS that extends from the conduction and valence band edges into the band gap. In a multitude of semiconductor materials, such as GaAs[36], c-Si[37], a-Si:H[1], CdTe[38], $CH_3NH_3PbI_3$[7], PbS[8], CuZnSn $(S_xSe_{1-x})_4$[4,39,40], and $CuInSe_2$[41,42], the extension of the DOS into the band gap follows an exponential energy dependence. In such a case, the band tails are labeled as Urbach tails.[43] Figure 1a illustrates an example of the DOS reaching exponentially into the band gap in a direct semiconductor. According to Cody et al[1] and John et al[44], Urbach tails are caused by phonons and by static disorder, that is, by lattice vibrations and defects, that lead to deviations from the perfect crystal lattice. In the case of CIGSe, origins of disorder and hence Urbach tails are likely to be related to variations in the bond lengths[45] and potential fluctuations of which there are two kinds: band gap fluctuations and electrostatic potential fluctuations.[2,46]

Band gap fluctuations in CIGSe arise from inhomogeneities in the elemental composition. As the band gap energy is most strongly influenced by the gallium content[47,48], local variations in the [Ga]/([Ga] + [In]) (GGI) ratio lead to local variations of the band gap energy.[49] Band gap fluctuations that are due to this alloy disorder are unavoidable. In addition to the Ga content, variations of the copper content also play a role as nonstoichiometry can lead to strain-induced fluctuations of the band edges.[46]

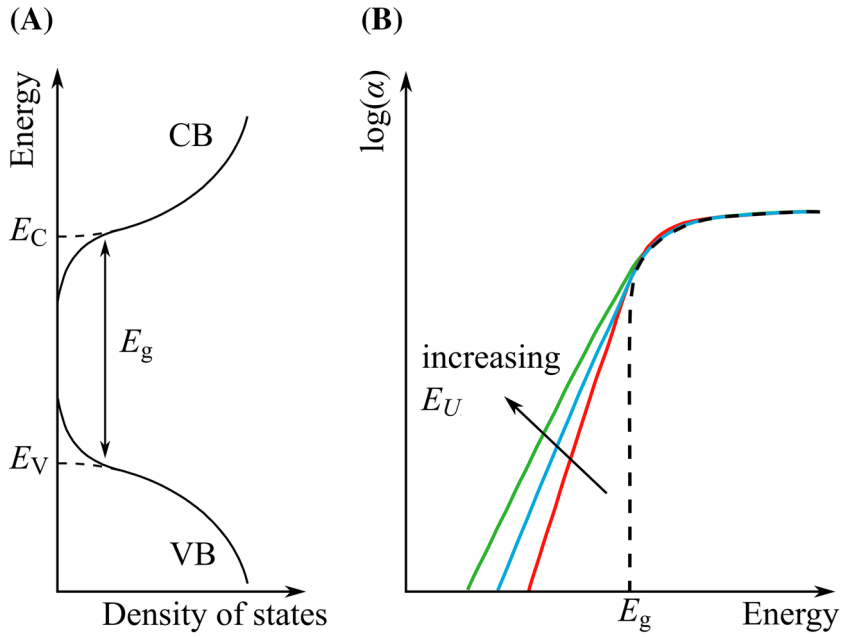

FIGURE 1 (a) In the case of an ideal direct semiconductor, the conduction band (CB) and valence band (VB) densities of states do not extend into the band gap (dashed lines). However, in the case of a real semiconductor, the density of states (DOS) may extend exponentially into the band gap and thus lead to states that are available for optical transitions (full lines). (b) Absorption coefficient α spectra of an ideal direct semiconductor (dashed lines) and of a real semiconductor (full lines). An exponentially decaying joint DOS leads to an absorption coefficient α that shares the same energetic dependence. Depending on how strongly the DOS extends into the band gap, the absorption coefficient shows a different decay below the band gap energy E_g, which is characterized by the Urbach energy E_U. The more the DOS extends into the band gap, the larger E_U and the more states are available for transitions. Above E_g, the absorption coefficient shows the classical square-root-like dependence on the photon energy [Colour figure can be viewed at wileyonlinelibrary.com]

Electrostatic potential fluctuations arise from local inhomogeneities of charged defects, which is a consequence of Cu-poor (i.e., state of the art) CIGSe being a compensated semiconductor. The randomly distributed charged defects exert a Coulomb potential onto the charge carriers in the bands, leading to fluctuations of the bands,[42,50,51] which however flatten at room temperature.[52,53] In addition, charged defects are known to accumulate at grain boundaries, leading to a band bending which is another source of disorder.[52,54]

The Urbach tails represent a joint DOS within the band gap that are available for optical transitions. With the absorption coefficient α being proportional to the joint DOS[2], the optical absorption edge replicates the characteristic exponential decay of the Urbach tails within the band gap. Figure 1b illustrates the absorption coefficient behavior in function of the photon energies involved. Above the band gap energy E_g, α follows the classical square root-like behavior (see, e.g.,[55]), while below E_g, α shows the Urbach-like exponential decay that is mathematically described as $\alpha \tilde{e}xp(\frac{E}{E_U})$ (see e.g.[56]). The amount of subband gap absorption can be described by the characteristic Urbach energy E_U: The larger E_U, the more the joint DOS extends into the band gap. In the case of Urbach energies E_U larger than 25 meV (i.e., k_BT), as is typically the case in kesterites[4], the QFLS is low as charge carriers populate tail states rather than the band edge. In systems where E_U is lower than 25 meV, band tails are generally assumed to be benign. Here, we investigate the influence of such "weak" tail states on the open-circuit voltage of the solar cells.

4 | RESULTS AND DISCUSSION

4.1 | Influence of alkali atoms on band tails in Cu(In,Ga)Se_2

To investigate the influence of the alkali atoms on the band tails in CIGSe, the absorption coefficient α spectra need to be measured. From the multiple experimental techniques that are able to determine α, we use photoluminescence spectroscopy (PL) as our main experimental technique since it allows for the detection of α over magnitude.[30,31] Extracting the absorption coefficient from photoluminescence spectra recorded at room temperature involves determining the QFLS and the absorptivity from the PL spectra, by analyzing them in terms on Planck's generalized law. An exponential fit to the low-energy slope of the absorption coefficient at energies significantly lowers than the band gap energy then enables us to extract the Urbach energy E_U. The detailed procedure is given in ref.[31] and in Section S2 of the supporting information. In this study, the Urbach energy is extracted from the low-energy slope of the

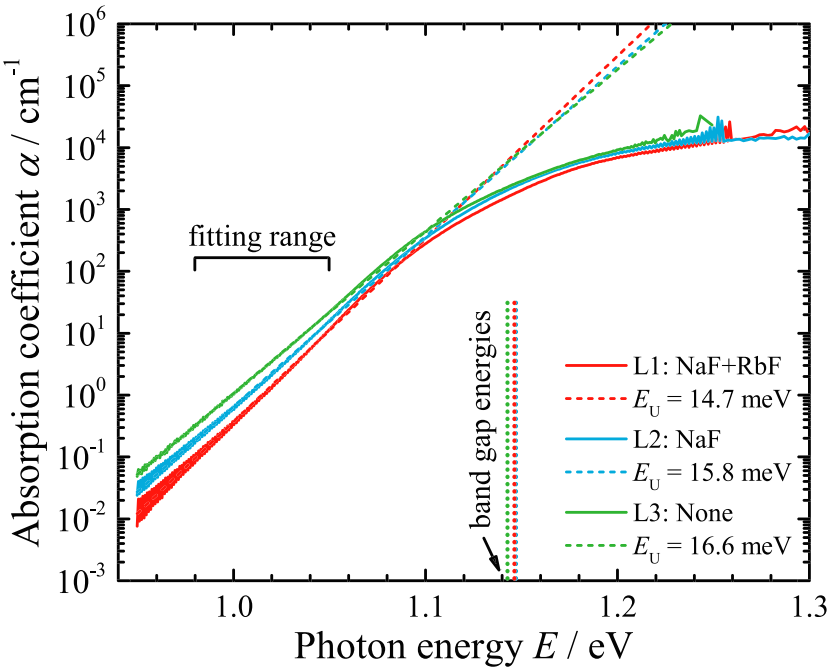

FIGURE 2 Absorption coefficient α spectra in semilogarithmic representation of the CdS-covered graded absorbers L1 (red curve), L2 (blue curve), and L3 (green curve). The dashed lines represent the fit applied in the indicated exemplary fitting range (0.98 to 1.05 eV) that yields the Urbach energies E_U as displayed in the bottom-right corner of the graph. The values of E_U depend only weakly on the exact fitting range. Also shown are the band gap energies (dotted lines) as indicated in Table 1 of Section 2. The determination of the band gap energies is explained in Section S1 of the supporting information [Colour figure can be viewed at wileyonlinelibrary.com]

absorption coefficient deep in the gap and not from the energy range just below the band gap, which can lead to unphysically high Urbach energies.[4,31]

Figure 2 shows the absorption coefficient spectra of the CdS-covered CIGSe absorbers L1 (with NaF and RbF-PDT—red curve), L2 (with NaF-PDT—blue curve), and L3 (without alkalis—green curve) in a semilogarithmic representation. For the fitting range specified in the graph, the exponential fits (dashed lines) yield an Urbach energy of 14.7 meV for sample L1, 15.8 meV for sample L2, and 16.6 meV for sample L3. These results thus clearly reveal a strong influence of the alkali atoms on the band tails: A reduction of the Urbach energy in the CIGSe absorber that contains Na (L2) compared to the one that does not contain any alkalis (L3). In addition, the presence of the heavier alkali atoms Rb (L1) leads to an additional decrease of the Urbach energy. In this specific example, the range over which the fit is done extends over 2 orders of magnitude in absorption coefficient which is only possible because the measurement extends over 4 orders of magnitude or more. The fitting range in Figure 2 is only one of multiple different fitting ranges that are selected for the extraction of E_U. Different fitting ranges lead to slightly different E_U (the exact influence is showcased in Figure S6 of the supporting information) which are used to perform a statistical analysis and identify a standard deviation. The standard deviation is then used to form the error bars in the following sections and figures. It can thus be concluded that the presence of alkali atoms within the CIGSe absorber leads to a reduction of the Urbach energy, that is, of the band tails. In ref.[9], the same observation was made through EQE measurements. Additionally, this reduction is stronger if a heavier alkali species such as Rb is present compared to a lighter species such as Na. It is likely that alkali accumulation at grain boundaries removes charged defects and thus band bending at the grain boundaries, as discussed in detail in ref[9]. The important point for the current study is that it is possible to manipulate the band tails in the same material.

4.2 | Influence of Cu content on band tails of Cu(In,Ga)Se2

To demonstrate that the band tails are strongly manipulated by the alkali treatments, we also study the dependence of the Urbach energy on the Cu content. As mentioned in Section 3, one origin of band tails can be electrostatic potential fluctuations that are present in state-of-the-art CIGSe absorbers. From literature reports, it is known that the magnitude of the electrostatic potential fluctuations decreases with increasing [Cu]/([Ga] + [In]) (CGI) ratio.[42,57] A recent related study, where a multitude of CIGSe solar cells with different alkali PDT processes were investigated, reveals a reduction of the band tails with increasing CGI ratio from 0.8 to 1.[22] Figure 3 shows the extracted Urbach energy E_U from photoluminescence in dependence of the CGI ratio for all the samples listed in Table 1. Generally, a slight expected trend is distinguishable as the band tails are reduced in samples that exhibit a higher CGI ratio. However, this trend is only clear for the samples grown at low temperatures (L1, L2, L3, LN1, LN2, and LS) and the LC sample. The samples grown at high temperatures, H1 and H2, do not follow this trend as their Urbach energies are considerably lower yet their CGI ratio is not higher compared to the other samples. Considering only the samples that were prepared under identical conditions but received different PDTs, that is, the samples that share the same label (i.e., L1–3, LN1–2, and H1–2), Figure 3 offers a very important conclusion: The presence of alkali atoms in the absorbers influences the band tails more than the CGI ratio.

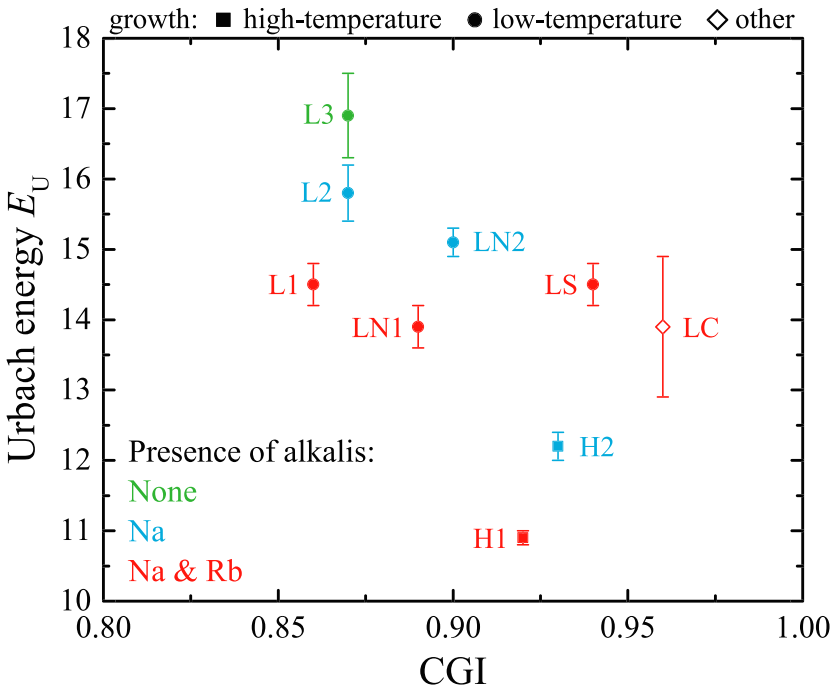

FIGURE 3 Urbach energy E_U as extracted from photoluminescence as a function of the absorber CGI ratio. The samples grown in a high-temperature process are displayed as squares while the samples grown in a low-temperature process are represented by circles. The sample LC is displayed by an open-diamond symbol. The color code alludes to the presence of alkalis in the samples and is explained in the bottom-left corner. The vertical error bars are extracted from a statistical analysis as described for Figure 2 [Colour figure can be viewed at wileyonlinelibrary.com]

4.3 | Correlation between band tails and voltage losses

The previous sections have shown that the presence of alkali atoms is an effective driver for the reduction of band tails in CIGSe absorbers and solar cells. Additionally, it is known from multiple published studies that the alkali atoms also lead to an increase of the optoelectronic quality of CIGSe solar cells through an increase in the open-circuit voltage V_{OC}.[14,22,33] These findings hint at a correlation between the V_{OC} and the Urbach energy E_U that has experimentally already been demonstrated in other materials.[5,6,8] Figure 4 shows the open-circuit voltage deficit with respect to the Shockley–Queisser limit $V_{OC}^{SQ} - V_{OC}$ of the samples investigated in this study in dependence of their extracted Urbach energies. Compared to the aforementioned studies[5,6,8], where the main figure of merit is the open-circuit voltage deficit $E_g - qV_{OC}$, the quantity $V_{OC}^{SQ} - V_{OC}$ is more accurate when representing materials with significantly different band gap energies. In this case, for matters of reference and comparison, some selected literature data for GaAs, c-Si, $CH_3NH_3PbI_3$, and CdTe are included in Figure 4 (triangle symbols). Additionally, different data sets are plotted for the reference technologies to show the possible variability of the selected parameters in literature. The inclusion of GaAs is motivated by the fact that it represents the single-junction solar cell technology with the highest efficiency[58] and can thus be used as a reference point. For the GaAs data point labeled (1), we selected the highest V_{OC} (from the record device, i.e., 1.1272 V[58]) and the lowest E_U (6.9 meV[36] from a single crystal) while the GaAs point labeled (2) represents a slightly inferior combination (taken from ref.[5] and references therein). In both cases, to compute V_{OC}^{SQ}, the band gap energy of 1.42 eV was used.[59] The inclusion of c-Si in Figure 4 is insightful because it shows that CIGSe solar cells can achieve a similar open-circuit voltage deficit while still exhibiting a lower power conversion efficiency. The c-Si data point labeled (3) represents the V_{OC} of the current champion device (0.738 V[58]) with the lowest published Urbach energy from a different crystal (9.6 meV[37]). The c-Si data point labeled (4) is taken from ref.[5] and references therein and shows that the location of the c-Si data point on the graph depends strongly on the various published Urbach energies. The value of 1.12 eV was used for the band gap of the c-Si data points.[59] The two perovskite data points labeled (5) are taken from the recent study by Ledinsky et al[6] while the data point (6) is taken from the older study by De Wolf et al[5] Finally, for the CdTe data point (7) we took the V_{OC} from the record device.[58] The band gap energy was extracted via linear extrapolation from the EQE curve that was given in ref.[60]. The CdTe Urbach energy was extracted from the study by Rakshani.[38] The inclusion of literature data is generally problematic as, in general, Urbach energy data are not reported for devices fabricated for photovoltaic purposes. Consequently, for the literature data we use V_{OC} loss and Urbach energy values from different samples, which will be at least partly responsible for some of the outliers to the general trend in Figure 4. The advantage of the new experimental data added in this study is that Urbach energies and V_{OC} losses have been determined on the same samples. Recently, a new study by Liu et al has revealed a record V_{OC} for a $CH_3NH_3PbI_3$ solar cell.[61] The inclusion of this data point in Figure 4 is discussed in Section S8 of the supporting information.

The data in Figure 4 exhibit a reduction of the voltage losses with decreasing Urbach energies. Using GaAs as a reference point, an empiric trend (gray dashed line) is observable that suggests that the voltage losses are caused by the Urbach tails. Only the c-Si data point (3) and the alkali-free L3 sample strongly deviate from this trend and show a V_{OC} loss higher than the one given by the trend with Urbach

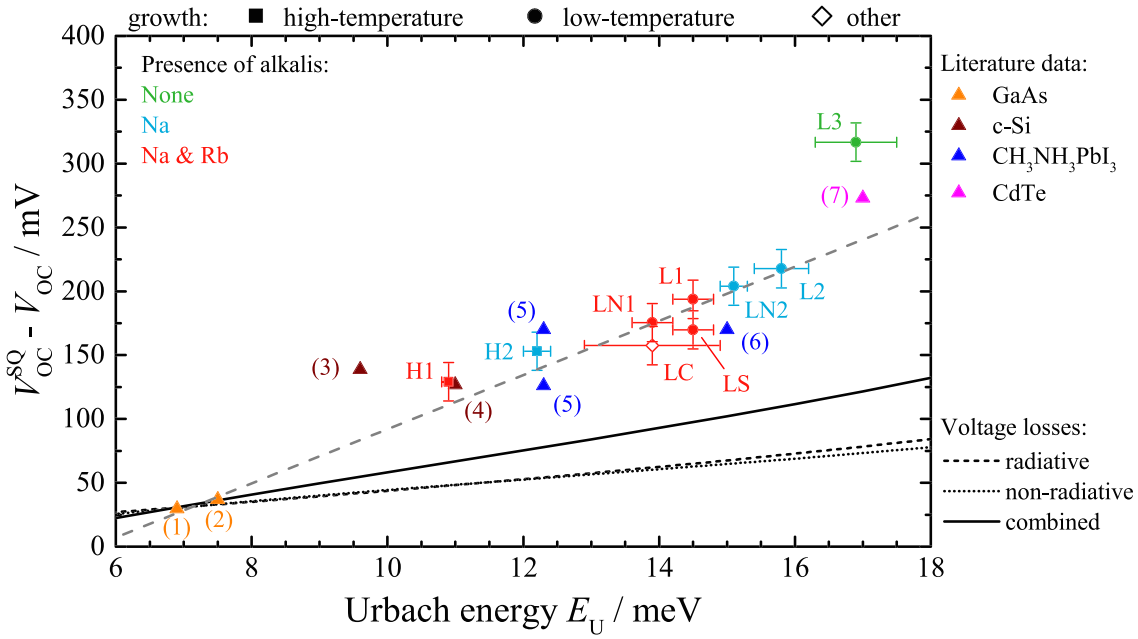

FIGURE 4 Open-circuit voltage deficit with respect to the SQ limit $V_{OC}^{SQ} - V_{OC}$ in dependence of the Urbach energy E_U of the samples investigated in this study. The square symbols represent the CIGSe samples grown at high temperatures, the circles the samples grown at low temperatures and the open-diamond symbol represents the LC sample. The color code alludes to the presence of alkali atoms and is explained in the top-left corner. The V_{OC} values were measured on the finished solar cell devices while E_U was extracted from the absorbers. Figure S7 of Section S4 in the supporting information shows the influence of E_U on the quasi-Fermi level splitting deficit and reveals a similar trend in the absorbers. The triangle symbols represent selected literature data for GaAs (1, 2), c-Si (3, 4), $CH_3NH_3PbI_3$ (5, 6), and CdTe (7) described in the text. Also shown are estimated voltage losses in case recombination processes are occurring via band tails through a radiative channel (dashed line), a nonradiative channel (dotted line), or a combination of both (continuous line), all offset to the GaAs data point (1) as it serves as reference. The gray dashed line is a guide to the eye and shows the empirical trend [Colour figure can be viewed at wileyonlinelibrary.com]

energies. The deviation of the c-Si data point (3) from the trend might be explained by the fact that we chose the lowest Urbach energy ever measured in c-Si for this data point. The c-Si data point (4) shows that even an indirect semiconductor can follow the empirical trend.

The trend observed in Figure 4 is also observed with QFLSs instead of open-circuit voltages (see Figure S7 and ref. [9]) with a very similar slope. The QFLS is determined from the PL spectra measured on the absorber before junction formation, that is, without the formation of a significant space-charge region. We have already previously demonstrated that the difference between QFLS and V_{OC} is very small (below 10 mV) in state-of-the-art Cu(In,Ga)Se_2 devices.[33] This observation indicates that the recombination mechanisms leading to the V_{OC} loss occur in the quasi-neutral region of the absorber, not in the space-charge region.

Band tails can contribute to voltage losses through both radiative and nonradiative recombination. First, we calculate the loss due to additional radiative recombination. As shown in Figure 1, band tails are states within the band gap that participate in absorption events. Consequently, the number of photons that can be absorbed is larger in a semiconductor with band tails than in an identical semiconductor without band tails. However, following the principle of detailed balance, states that lead to absorption processes also lead to emission processes in thermal equilibrium.[62] Thus, the presence of sub band gap states leads to an increase in the radiative equilibrium recombination which, in turn, leads to a reduction of the open-circuit voltage. Charge carriers thermalize into the tail states and lose energy in the process. Thus, these recombination processes are transitions where at least one of the states (initial and/or final) is a carrier trapped in a tail state. To estimate the voltage losses through radiative band tail recombination, we modify the Shockley–Queisser model[63] to allow for absorption and emission from Urbach tails (labeled in the following Shockley–Queisser–Urbach [SQU] model). This is done by defining the following absorption coefficient[56]

$$\alpha(E) = \begin{cases} \alpha_0 \exp\left(-\frac{E_0 - E}{E_U}\right) & ,\text{for } E < E_g \\ \alpha_0 & ,\text{for } E \geq E_g, \end{cases} \quad (1)$$

where α_0 and E_0 are material-specific parameters. For reasons of simplicity, we set $E_0 = E_g$. Additionally, to ensure that the absorptivity equals unity above E_g, as assumed in the Shockley–Queisser model, we set α_0 to $10^5\,cm^{-1}$. The latter is a strong simplification as the absorption coefficient follows a square root behavior at energies above the band gap energy.[55] It should be noted that Equation 1 is a useful approximation for the absorption behavior of tail states to calculate voltage losses only in the case of Urbach energies smaller than k_BT. For higher Urbach energies, the fact that $\alpha(E)$ changes with the occupation of states, that is, with the position of the quasi-Fermi

levels, needs to be taken into account.[64,65] From the absorption coefficient, the absorptivity $a(E)$ can be determined through the simplified expression[28]

$$a(E) = 1 - \exp(-\alpha(E)d), \tag{2}$$

where we assume the absorber thickness d to be 2.5 μm. Using the whole absorber thickness here is a simplification since the emission is not from the whole absorber but just from the notch region around the band gap minimum.[33] The error is negligible with respect to the other simplifications made here. Compared to the Shockley–Queisser model where a step function for $a(E)$ is assumed, Expression 2 is slightly larger than 0 below E_g and slightly below unity above it. Equation 2 is inserted into the well-known expressions for the short-circuit current density j_{SC}^{SQU} and saturation current density j_0^{SQU}:[66,67]

$$j_{SC}^{SQU} = q\int_0^\infty a(E)\cdot\Phi_{sun}(E)\,dE, \tag{3}$$

$$j_0^{SQU} = q\int_0^\infty a(E)\cdot\Phi_0(E,T)\,dE. \tag{4}$$

The quantity $\Phi_{sun}(E)$ represents the photon flux density of the AM1.5 spectrum, while the quantity $\Phi_0(E,T)$ describes the thermal black body photon flux density, where we use a temperature T of 296 K. The current densities are determined by numerical integration. Finally, both short-circuit and saturation current densities are inserted into the open-circuit voltage expression of the SQ model

$$V_{OC}^{SQU} = \frac{k_B T}{q}\ln\left(\frac{j_{SC}^{SQU}}{j_0^{SQU}} + 1\right). \tag{5}$$

The exact details, parameters, and restrictions of the SQU model are described in Section S5 of the supporting information. Since we want to compare with real world open-circuit voltages, we calculate the decrease of V_{OC}^{SQU} with increasing Urbach energy using the GaAs data (1) in Figure 4 as the reference point. According to these calculations, represented by the black dashed line in Figure 4, an increase of the Urbach energy from 10 to 15 meV leads to an increased voltage loss of approximately 24 mV which is not negligible but also not significant enough to explain the observed losses. Similar calculations in literature show very similar voltage losses for the Urbach energy region under investigation.[8,68]

In addition to radiative recombination processes, states within the band gap also participate in nonradiative recombination processes of the Shockley–Read–Hall (SRH) type.[69,70] Contrary to the radiative recombination process where at least one of the states is a carrier trapped in a tail state, the SRH recombination process considers the recombination of free carriers where the initial and final states are an extended band state. While the probability of SRH recombination processes increases the more the states are situated between the demarcation levels (i.e., close to mid gap)[71], nonradiative recombination processes can also occur through states close to the band edges.[59] To estimate the voltage losses in a p-type semiconductor that are resulting from nonradiative band tail recombination, we equated the band tails with a defect density $N(E_T)$ that has a peak defect density N_0 at the conduction band minimum E_C and decays exponentially into the band gap according to

$$N(E_T) = N_0\,\exp\left(-\frac{E_C - E_T}{E_U}\right) \tag{6}$$

with E_T being the energy of the tail state. For the DOS given in Equation 6, the nonradiative recombination rate of free carriers in the bands can be calculated through the SRH recombination rate[69,70]

$$R_{SRH} = \frac{np - n_0 p_0}{(n+n^*)\tau_p + (p+p^*)\tau_n}, \tag{7}$$

with n and p the free carrier concentrations of electrons and holes, respectively, and $n^* = N_C\exp[\frac{E_T - E_C}{k_B T}]$ and $p^* = N_V\exp[\frac{E_V - E_T}{k_B T}]$ the auxiliary charge carrier densities. The lifetimes $\tau_{n/p}$ are expressed as $\tau_{n/p} = [\sigma_{n/p} v_{th} N(E_T)]^{-1}$ where v_{th} is the thermal velocity and $\sigma_{n/p}$ is the recombination cross section for electrons and holes, respectively. By assuming the recombination cross-section to be equal for both electrons and holes, the SRH recombination rate can be written as follows

$$R_{SRH}(E_T) = \sigma v_{th} N(E_T)\frac{np - n_i^2}{n+n^*+p+p^*}. \tag{8}$$

For tail states with Urbach energies smaller than $k_B T$, the auxiliary charge carrier densities are always considerably higher than n or p. Thus, we end up with the expression (the detailed arguments are given in Section S6 of the supporting information)

$$R_{SRH}(E_T) = \sigma v_{th} np\frac{N_0}{N_C}\exp\left(\frac{E_T - E_C}{E_R}\right), \tag{9}$$

with the quantity E_R being the decay energy of the SRH recombination rate that is a consequence of the decaying nature of the recombination activity of tail states with decay energy E_U according to

$$\frac{1}{E_R} = \frac{1}{E_U} - \frac{1}{k_B T}. \tag{10}$$

It is obvious from Equation 10 that the approximations we make here work only for Urbach energies smaller than $k_B T$. The other parameters needed to calculate absolute values to R_{SRH} are not known. Therefore, we calculate only the increase of the open-circuit loss $\Delta\Delta V_{OC}^{nrad}$ as the Urbach energy increases. As explained in detail in @Section S6 of the supporting information, the increase $\Delta\Delta V_{OC}^{nrad}$ in open-circuit voltage loss following an increase of the Urbach energy E_U in the case of nonradiative tail recombination is mostly dictated by the decay energy E_R via

$$\Delta\Delta V_{OC}^{nrad} \approx \frac{k_B T}{q} \ln\left(\frac{E_R^B}{E_R^A}\right), \quad (11)$$

where E_R^A constitutes the reference decay energy. Choosing, for example, as reference value an Urbach energy of 10 meV, the reference SRH recombination rate decay energy E_R^A would equate to 16.4 meV according to Equation 10. Increasing the Urbach energy to 15 meV would then lead to an SRH recombination rate decay energy E_R^B of 36.4 meV. Such an increase in the Urbach energy finally leads to an increase in the nonradiative voltage loss $\Delta\Delta V_{OC}^{nrad}$ of approximately 20 mV according to Equation 11. For a broader Urbach energy range, the nonradiative voltage losses are represented by the dotted black line in Figure 4 as well as in Figure S10 in the supporting information. In Section S7 of the supporting information, we present the results from SCAPS simulations where near-identical results are obtained. Finally, it is important to mention that the above calculations are only based on the presence of a conduction band tail (cf. Equation 6). However, since electrons are the minority charge carriers in a p-type semiconductor, the inclusion of an additional valence band tail does not influence the calculated results. From the dotted black line in Figure 4, we see that the voltage losses due to nonradiative recombination are similar in magnitude to the radiative losses and can, thus, also not explain the observed trend.

The losses due to radiative recombination through tail states and due to nonradiative recombination via tail states are of the same magnitude. This might be surprising in two ways. Firstly, for inorganic semiconductors the radiative loss can be usually neglected with respect to the nonradiative loss.[67] However, the tail states will increase radiative recombination significantly, since states at lower energies contribute more due to the exponential increase of the black body photon flux density Φ_0 that enters into Equation 4. Our model covers the tail states deep down into the band gap. And the modeled nonradiative loss is due to SRH recombination through states near the band edges, which do not contribute as much as deep states. Thus, secondly, it may seem surprising that states so close to the edges lead at all to a nonradiative recombination loss. Das et al. recently investigated the recombination activity of defects as function of their energy in the band gap and found that only defects near midgap contribute significantly to nonradiative recombination.[72] However, assuming a defect density of 10^{15} cm^{-3}, they find a nonradiative lifetime for defects near the band edges of about 100 ms, for a range of different semiconductors. The DOS in the band tails is certainly much higher, in the order of the effective DOS in the band. With about 4 orders of magnitude higher DOS, the nonradiative lifetime, only due to tail states, is in the same range as the radiative lifetime. Thus, a comparable voltage loss due nonradiative recombination via the tail states and due to radiative recombination through tail states is to be expected.

Since both radiative and nonradiative recombination processes occur simultaneously, the continuous black line in Figure 4 visualizes the total expected voltage loss due to band tail recombination, which is obtained by summing up the radiative and nonradiative voltage losses. The comparison between the measured data and the calculated losses indicates that band tails lead to about a factor of 2 more V_{OC} loss than expected from radiative and SRH recombination processes and appear to contribute to the losses via an additional (nonradiative) channel. One possible nature of this additional channel could be nonlocal recombination processes through tails that involve tunneling of electrons and holes, for example, in the band bending around charged extended defects. The additional recombination has to be a mechanism that does not depend on the details of the material, as we observe a general correlation between band tails and voltage losses across a broad spectrum of technologies in Figure 4 and in previous studies.[5,6,8] The fact that voltage losses correlate so well to the Urbach energy across a wide variety of technologies strongly hints at a causal relationship: Recombination through tail states appears to limit the open-circuit voltage in state-of-the-art photovoltaic devices. This effect is worse than expected from the influence of tail states on radiative and SRH recombination.

5 | CONCLUSION

Since band tails constitute a DOS that extend into the band gap, they induce additional radiative and nonradiative recombination channels that contribute to losses in the open-circuit voltage V_{OC} of solar cell devices. The correlation between voltage losses and Urbach energy has recently been investigated for various solar cell technologies. Empirically, a linear trend between V_{OC} loss and the Urbach energy has been demonstrated in the literature. Alkali treatments on state-of-the-art thin-film Cu(In,Ga)Se_2 absorbers with efficiencies of 20% and above allow to manipulate the amount of tailing, as measured by the Urbach energy through photoluminescence and photocurrent spectroscopy. We determined the open-circuit voltage loss and the Urbach energy in the same sample. The relation of the voltage deficit with respect to the theoretical Shockley–Queisser limit in dependence of the Urbach energy for various solar cell technologies confirms the previously observed empirical trend: a linear reduction of the voltage losses in devices that show weaker band tails. We implemented two theoretical models that account for the voltage losses through both radiative and SRH nonradiative band tail recombination: Radiative recombination is increased because the carriers that thermalize into the tail states can recombine radiatively; nonradiative recombination removes carriers from the extended band states via SRH recombination through the tail states. Through the models, we demonstrate that, in fact, an increase in Urbach energy of only 1 meV leads to an increase in voltage loss as high as 10 mV. The modeled contributions of radiative and nonradiative recombination to the additional voltage loss are about 5 mV each. However, the measured voltage losses turn out to be more severe by a factor of 2 compared to the theoretically predicted ones. Consequently, an additional (nonradiative) loss mechanism must be active in these devices that go beyond straightforward SRH recombination. Given the generality of the empirical trend, we suggest that band tails are also responsible for this additional voltage loss, possibly through nonlocal recombination

processes involving the tunneling of electrons and holes. Thus, we conclude that the recombination through tail states is the main cause of the voltage loss in these state-of-the art devices. This loss is accounted for to 25% by radiative recombination, to 25% by SRH recombination, and to 50% by an additional nonradiative mechanism that is not understood yet. It appears that band tails are the main driver for open-circuit voltage losses in the majority of state-of-the-art solar cell technologies.

ACKNOWLEDGMENTS

This work was financially supported in part by the European Union's Horizon 2020 research and innovation program under Grant 641004 (Sharc25) and in part by the Swiss State Secretariat for Education, Research and Innovation (SERI) under Contract number 15.0158. The authors thank Marc Burgelman (Ghent University) for very helpful and fruitful discussions.

ORCID

Max Hilaire Wolter https://orcid.org/0000-0002-9202-7627
Benjamin Bissig https://orcid.org/0000-0001-9066-027X

REFERENCES

1. Cody GD, Tiedje T, Abeles B, Moustakas TD, Brooks B, Goldstein Y. *J Phys Colloques*. 1981;42:C4-301-C4-304.
2. Pankove JI. *Optical Processes in Semiconductors*. New-York: Dover Publications; 1971.
3. Chantana J, Nishimura T, Kawano Y, Teraji S, Watanabe T, Minemoto T. Examination of relationship between urbach energy and open-circuit voltage deficit of flexible Cu(In,Ga)Se_2 solar cell for its improved photovoltaic performance. *ACS Appl Energy Mater*. 2019;2(11):7843-7849.
4. Rey G, Larramona G, Bourdais S, et al. On the origin of band-tails in kesterite. *Solar Energy Materials and Solar Cells*. 2018;179:142-151.
5. De Wolf S, Holovsky J, Moon S-J, et al. Organometallic halide perovskites: sharp optical absorption edge and its relation to photovoltaic performance. *J Phys Chem Lett*. 2014;5(6):1035-1039.
6. Ledinsky M, Schönfeldová T, Holovský J, et al. Temperature dependence of the Urbach energy in lead iodide perovskites. *J. Phys. Chem. Lett.* 2019;10(6):1368-1373.
7. Zhang W, Saliba M, Moore DT, et al. Ultrasmooth organic–inorganic perovskite thin-film formation and crystallization for efficient planar heterojunction solar cells. *Nat Commun*. 2015;6(1):6142-6151.
8. Jean J, Mahony TS, Bozyigit D, et al. Radiative efficiency limit with band tailing exceeds 30% for quantum dot solar cells. *ACS Energy Lett*. 2017;2(11):2616-2624.
9. Siebentritt S, Avancini E, Bär M, et al. Heavy alkali treatment of Cu(In,Ga)Se_2 solar cells: surface versus bulk effects. *Adv. Energy Mater.* 2020;10(8):1903752, 1-15.
10. Rudmann D, da Cunha AF, Kaelin M, et al. Efficiency enhancement of Cu(In,Ga)Se_2 solar cells due to post-deposition Na incorporation. *Appl Phys Lett*. 2004;84(7):1129-1131.
11. Jackson P, Hariskos D, Lotter E, et al. New world record efficiency for Cu(In,Ga)Se_2 thin-film solar cells beyond 20%. *Prog. Photovolt: Res. Appl.* 2011;19(7):894-897.
12. Nakamura M, Yamaguchi K, Kimoto Y, Yasaki Y, Kato T, Sugimoto H. Cd-free Cu(In,Ga)(Se,S)2 thin-film solar cell with record efficiency of 23.35%. *IEEE J. Photovoltaics*. 2019;9(6):1863-1867.
13. Chirilă A, Reinhard P, Pianezzi F, et al. Potassium-induced surface modification of Cu(In,Ga)Se_2 thin films for high-efficiency solar cells. *Nature Mater*. 2013;12(12):1107-1111.
14. Jackson P, Wuerz R, Hariskos D, Lotter E, Witte W, Powalla M. Effects of heavy alkali elements in Cu(In,Ga)Se_2 solar cells with efficiencies up to 22.6%. *Phys. Status Solidi RRL*. 2016;10(8):583-586.
15. Kato T, Wu J-L, Hirai Y, Sugimoto H, Bermudez V. Record efficiency for thin-film polycrystalline solar cells up to 22.9% achieved by Cs-treated Cu(In,Ga)(Se,S)2. *IEEE J Photovoltaics*. 2019;9(1):325-330.
16. Handick E, Reinhard P, Alsmeier J-H, et al. Potassium postdeposition treatment-induced band gap widening at Cu(In,Ga)Se_2 surfaces—reason for performance leap? *ACS Appl Mater Interfaces*. 2015;7(49):27414-27420.
17. Heinemann MD, Kodalle T, Hages C, et al. Evaluation of recombination losses in thin film solar cells using an LED sun simulator—the effect of RbF post-deposition on CIGS solar cells. *EPJ Photovolt*. 2018;9:9-14.
18. Pianezzi F, Reinhard P, Chirilă A, et al. Unveiling the effects of post-deposition treatment with different alkaline elements on the electronic properties of CIGS thin film solar cells. *Phys Chem Chem Phys*. 2014;16(19):8843-8851.
19. Pistor P, Greiner D, Kaufmann CA, et al. Experimental indication for band gap widening of chalcopyrite solar cell absorbers after potassium fluoride treatment. *Appl Phys Lett*. 2014;105(6):063901, 1-4.
20. Kodalle T, Heinemann MD, Greiner D, et al. Elucidating the mechanism of an RbF post deposition treatment in CIGS thin film solar cells. *Sol RRL*. 2018;2(9):1800156, 1-9.
21. Avancini E, Carron R, Weiss TP, et al. Effects of rubidium fluoride and potassium fluoride postdeposition treatments on Cu(In,Ga)Se_2 thin films and solar cell performance. *Chem Mater*. 2017;29(22):9695-9704.
22. Carron R, Nishiwaki S, Feurer T, et al. Advanced alkali treatments for high-efficiency Cu(In,Ga)Se_2 solar cells on flexible substrates. *Adv Energy Mater*. 2019;9(24):1900408, 1-8.
23. Friedlmeier TM, Jackson P, Bauer A, et al. High-efficiency Cu(In,Ga)Se_2 solar cells. *Thin Solid Films*. 2017;633:13-17.
24. Chirilă A, Buecheler S, Pianezzi F, et al. Highly efficient Cu(In,Ga)Se_2 solar cells grown on flexible polymer films. *Nature Mater*. 2011;10(11):857-861.
25. Nishiwaki S, Feurer T, Bissig B, et al. Precise Se-flux control and its effect on Cu(In,Ga)Se 2 absorber layer deposited at low substrate temperature by multi stage co-evaporation. *Thin Solid Films*. 2017;633:18-22.
26. Weiss TP, Carron R, Wolter MH, et al. Time-resolved photoluminescence on double graded Cu(In,Ga)Se_2—impact of front surface recombination and its temperature dependence. *Science and Technology of Advanced Materials*. 2019;20(1):313-323.
27. Feurer T, Fu F, Weiss TP, et al. RbF post deposition treatment for narrow bandgap Cu(In,Ga)Se_2 solar cells. *Thin Solid Films*. 2019;670:34-40.
28. Würfel P. *Physics of Solar Cells*. Wiley-VCH Verlag GmbH & KGaA; 2005.
29. Gütay L, Bauer GH. Local fluctuations of absorber properties of Cu(In,Ga)Se_2 by sub-micron resolved PL towards "real life" conditions. *Thin Solid Films*. 2009;517(7):2222-2225.
30. Daub E, Würfel P. Ultralow values of the absorption coefficient of Si obtained from luminescence. *Phys Rev Lett*. 1995;74(6):1020-1023.
31. Rey G, Spindler C, Babbe F, et al. Absorption coefficient of a semiconductor thin film from photoluminescence. *Phys Rev Applied*. 2018;9(6):064008, 1-11.
32. Wolter MH, Bissig B, Reinhard P, Buecheler S, Jackson P, Siebentritt S. *Phys. Status Solidi C*. 2017:1600189, 1-4.
33. Wolter MH, Bissig B, Avancini E, et al. Influence of sodium and rubidium postdeposition treatment on the quasi-fermi level splitting of Cu(In,Ga)Se_2 thin films. *IEEE J. Photovoltaics*. 2018;8(5):1320-1325.
34. Wolter M.H., Siopa D., Lomuscio A., Weiss T.P., Thiele P., Dale P.J., Carron R., Avancini E., Bissig B., Buecheler S., Jackson P., Witte W., and Siebentritt S., In Preparation (n.d.).

35. Wolter MH. *Optical Investigation of Voltage Losses in High-Efficiency Cu (In,Ga)Se_2 Thin-Film Solar Cells*. University of Luxembourg; 2019 http://hdl.handle.net/10993/39611
36. Sturge MD. Optical absorption of gallium arsenide between 0.6 and 2.75 eV. *Phys. Rev.* 1963;129(6):768-773.
37. Cody GD. Urbach edge of crystalline and amorphous silicon: a personal review. *J Non Cryst Solids*. 1992;141:3-15.
38. Rakhshani AE. Heterojunction properties of electrodeposited CdTe/CdS solar cells. *J Appl Phys*. 2001;90(8):4265-4271.
39. Gokmen T, Gunawan O, Todorov TK, Mitzi DB. Band tailing and efficiency limitation in kesterite solar cells. *Appl Phys Lett*. 2013;103(10): 103506, 1-5.
40. Siebentritt S, Rey G, Finger A, et al. What is the bandgap of kesterite? *Solar Energy Materials and Solar Cells*. 2016;158:126-129.
41. Shioda T, Chichibu S, Irie T, Nakanishi H, Kariya T. Influence of non-stoichiometry on the Urbach's tails of absorption spectra for $CuInSe_2$ single crystals. *J Appl Phys*. 1996;80(2):1106-1111.
42. Siebentritt S, Gütay L, Regesch D, Aida Y, Deprédurand V. Why do we make Cu(In,Ga)Se_2 solar cells non-stoichiometric? *Solar Energy Materials and Solar Cells*. 2013;119:18-25.
43. Urbach F. The long-wavelength edge of photographic sensitivity and of the electronic absorption of solids. *Phys. Rev.* 1953;92(5):1324
44. John S, Soukoulis C, Cohen MH, Economou EN. Theory of electron band tails and the Urbach optical-absorption edge. *Phys Rev Lett*. 1986;57(22):1777-1780.
45. Schnohr CS, Eckner S, Schöppe P, et al. Reversible correlation between subnanoscale structure and Cu content in co-evaporated Cu(In,Ga)Se_2 thin films. *Acta Mater*. 2018;153:8-14.
46. Werner JH, Mattheis J, Rau U. *Thin Solid Films*. 2005;480–481: 399-409.
47. Alonso MI, Garriga M, Durante Rincón CA, Hernández E, León M. Optical functions of chalcopyrite CuGa x In 1-x Se 2 alloys. *Applied Physics A: Materials Science & Processing*. 2002;74(5):659-664.
48. Carron R, Avancini E, Feurer T, et al. Refractive indices of layers and optical simulations of Cu(In,Ga)Se_2 solar cells. *Science and Technology of Advanced Materials*. 2018;19(1):396-410.
49. Rau U, Werner JH. Radiative efficiency limits of solar cells with lateral band-gap fluctuations. *Appl Phys Lett*. 2004;84(19):3735-3737.
50. Shklovskij BI, Efros AL. *Electronic Properties of Doped Semiconductors*. Berlin: Springer-Verlag; 1984.
51. Yu PW. Excitation-dependent emission in Mg-, Be-, Cd-, and Zn-implanted GaAs. *J Appl Phys*. 1977;48(12):5043-5051.
52. Schmidt SS, Abou-Ras D, Sadewasser S, Yin W, Feng C, Yan Y. Electrostatic potentials at Cu(In,Ga)Se_2 grain boundaries: experiment and simulations. *Phys Rev Lett*. 2012;109(9):095506, 1-5.
53. Abou-Ras D, Schmidt SS, Schäfer N, et al. Compositional and electrical properties of line and planar defects in Cu(In,Ga)Se_2 thin films for solar cells—a review. *Phys Status Solidi RRL*. 2016;10(5): 363-375.
54. Kittel C. *Introduction to Solid State Physics*. Inc.: John Wiley & Sons; 2005.
55. Klingshirn CF. *Semiconductor Optics*. Berlin Heidelberg: Springer-Verlag; 2012.
56. Dirnstorfer I, Wagner M, Hofmann DM, Lampert MD, Karg F, Meyer BK. Characterization of CuIn(Ga)Se_2 thin films. *Physica Status Solidi (a)*. 1998;168(1):163-175.
57. Green MA, Dunlop ED, Hohl-Ebinger J, Yoshita M, Kopidakis N, Hao X. Solar cell efficiency tables (version 56). *Prog Photovolt Res Appl*. 2020;28(7):629-638.
58. Sze SM, Ng KK. *Physics of Semiconductor Devices*. New Jersey: John Wiley & Sons, Inc.; 2007.
59. Green MA, Emery K, Hishikawa Y, Warta W, Dunlop ED. Solar cell efficiency tables (Version 45). *Prog Photovolt: Res Appl*. 2015;23(1): 1-9.
60. Liu Z, Krückemeier L, Krogmeier B, et al. Open-circuit voltages exceeding 1.26 V in planar methylammonium lead iodide perovskite solar cells. *ACS Energy Lett*. 2019;4(1):110-117.
61. Bridgman PW. Note on the principle of detailed balancing. *Phys. Rev.* 1928;31(1):101-102.
62. Shockley W, Queisser HJ. Detailed balance limit of efficiency ofp-n junction solar cells. *J Appl Phys*. 1961;32(3):510-519.
63. Moore JE, Hages CJ, Agrawal R, Lundstrom MS, Gray JL. The importance of band tail recombination on current collection and open-circuit voltage in CZTSSe solar cells. *Appl Phys Lett*. 2016;109(2): 021102, 1-4.
64. van Berkel C, Powell MJ, Franklin AR, French ID. Quality factor ina-Si: Hnipandpindiodes. *J Appl Phys*. 1993;73(10):5264-5268.
65. Kirchartz T, Rau U. What makes a good solar cell? *Adv. Energy Mater.* 2018;8(28):1703385, 1-19.
66. Rau U, Blank B, Müller TCM, Kirchartz T. Efficiency potential of photovoltaic materials and devices unveiled by detailed-balance analysis. *Phys. Rev. Applied*. 2017;7(4):044016, 1-9.
67. Mattheis J, Rau U, Werner JH. Light absorption and emission in semiconductors with band gap fluctuations—a study on Cu(In,Ga)Se_2 thin films. *J Appl Phys*. 2007;101(11):113519, 1-11.
68. Hall RN. Electron-hole recombination in germanium. *Phys Rev*. 1952; 87(2):387
69. Shockley W, Read WT. Statistics of the recombinations of holes and electrons. *Phys. Rev.* 1952;87(5):835-842.
70. Simmons JG, Taylor GW. Nonequilibrium steady-state statistics and associated effects for insulators and semiconductors containing an arbitrary distribution of traps. *Phys Rev B*. 1971;4(2):502-511.
71. Das B, Aguilera I, Rau U, Kirchartz T. What is a deep defect? Combining Shockley-Read-Hall statistics with multiphonon recombination theory. *Physical Review Materials*. 2020;4(2):024602, 1-14.
72. Larsen JK, Burger K, Gutay L, Siebentritt S. *in 2011 37th IEEE Photovoltaic Specialists Conference*. WA, USA: IEEE, Seattle; 2011 pp. 000396–000401.

SUPPORTING INFORMATION

Additional supporting information may be found online in the Supporting Information section at the end of this article.

How to cite this article: Wolter MH, Carron R, Avancini E, et al. How band tail recombination influences the open-circuit voltage of solar cells. *Prog Photovolt Res Appl*. 2021;1-11. https://doi.org/10.1002/pip.3449